Developmental Biology 386 (2014) 395–407

Contents lists available at ScienceDirect

Developmental Biology

journal homepage: www.elsevier.com/locate/developmentalbiology

Reduced Euchromatin histone methyltransferase 1 causes developmental delay, hypotonia, and cranial abnormalities associated with increased bone gene expression in Kleefstra syndrome mice

Monique C.M. Balemans [a,b], Muhammad Ansar [a,c], Astrid R. Oudakker [a,d], Arjan P.M. van Caam [e], Brenda Bakker [e], Elly L. Vitters [e], Peter M. van der Kraan [e], Diederik R.H. de Bruijn [a], Sanne M. Janssen [a], Arthur J. Kuipers [b], Manon M.H. Huibers [b], Eliza M. Maliepaard [b], X. Frank Walboomers [f], Marco Benevento [d], Nael Nadif Kasri [d], Tjitske Kleefstra [a], Huiqing Zhou [a,g], Catharina E.E.M. Van der Zee [b,*,1], Hans van Bokhoven [a,d,1]

[a] Department of Genetics, Nijmegen Centre for Molecular Life Sciences, Radboud University Medical Centre, PO Box 9101, 6500 HB Nijmegen, The Netherlands
[b] Department of Cell Biology, Nijmegen Centre for Molecular Life Sciences, Radboud University Medical Centre, PO Box 9101, 6500 HB Nijmegen, The Netherlands
[c] Advance Centre of Biomedical Sciences, King Edward Medical University, Lahore, Pakistan
[d] Department of Cognitive Neurosciences, Donders Institute for Brain, Cognition and Behaviour, Radboud University Medical Centre, PO Box 9101, 6500 HB Nijmegen, The Netherlands
[e] Department of Rheumatology, Nijmegen Centre for Molecular Life Sciences, Radboud University Medical Centre, PO Box 9101, 6500 HB Nijmegen, The Netherlands
[f] Department of Biomaterials, Dentistry, Radboud University Medical Centre, PO Box 9101, 6500 HB Nijmegen, The Netherlands
[g] Department of Molecular Developmental Biology, Nijmegen Centre for Molecular Life Sciences, Radboud University Nijmegen, PO Box 9101, 6500 HB Nijmegen, The Netherlands

ARTICLE INFO

Article history:
Received 13 December 2012
Received in revised form
6 December 2013
Accepted 11 December 2013
Available online 19 December 2013

Keywords:
Postnatal development
Ehmt1 heterozygous knockout mice
Ehmt1
GLP
G9a-like protein
KMT1D
H3K9
Dimethylation
Skull and nose bone
mRNA
Runx2
Col11a
Col22a
Dmp1

ABSTRACT

Haploinsufficiency of Euchromatin histone methyltransferase 1 (EHMT1), a chromatin modifying enzyme, is the cause of Kleefstra syndrome (KS). KS is an intellectual disability (ID) syndrome, with general developmental delay, hypotonia, and craniofacial dysmorphisms as additional core features. Recent studies have been focused on the role of EHMT1 in learning and memory, linked to the ID phenotype of KS patients. In this study we used the *Ehmt1*$^{+/-}$ mouse model, and investigated whether the core features of KS were mimicked in these mice. When comparing *Ehmt1*$^{+/-}$ mice to wildtype littermates we observed delayed postnatal growth, eye opening, ear opening, and upper incisor eruption, indicating a delayed postnatal development. Furthermore, tests for muscular strength and motor coordination showed features of hypotonia in young *Ehmt1*$^{+/-}$ mice. Lastly, we found that *Ehmt1*$^{+/-}$ mice showed brachycephalic crania, a shorter or bent nose, and hypertelorism, reminiscent of the craniofacial dysmorphisms seen in KS. In addition, gene expression analysis revealed a significant upregulation of the mRNA levels of *Runx2* and several other bone tissue related genes in P28 *Ehmt1*$^{+/-}$ mice. Runx2 immunostaining also appeared to be increased. The mRNA upregulation was associated with decreased histone H3 lysine 9 dimethylation (H3K9me2) levels, the epigenetic mark deposited by Ehmt1, in the promoter region of these genes. Together, *Ehmt1*$^{+/-}$ mice indeed recapitulate KS core features and can be used as an animal model for Kleefstra syndrome. The increased expression of bone developmental genes in the *Ehmt1*$^{+/-}$ mice likely contributes to their cranial dysmorphisms and might be explained by diminished Ehmt1-induced H3K9 dimethylation.

Introduction

Kleefstra syndrome (KS) is a recently defined intellectual disability (ID) syndrome, caused by haploinsufficiency of the *Euchromatin histone methyltransferase 1* (*EHMT1*) gene (Kleefstra et al., 2006, 2009, 2010, 2012). Mouse Ehmt1/GLP/KMT1D forms

* Corresponding author.
E-mail address: i.vanderzee@ncmls.ru.nl (C.E.E.M. Van der Zee).
[1] These authors contributed equally to this work.

0012-1606/$ - see front matter © 2013 Elsevier Inc. All rights reserved.
http://dx.doi.org/10.1016/j.ydbio.2013.12.016

a heteromeric complex with Ehmt2/G9a/KMT1C to catalyze mono- and dimethylation of lysine 9 of the histone H3 N-terminal tail in euchromatic areas (H3K9me2) (Tachibana et al., 2005), which is an epigenetic mark for transcriptional silencing (He and Lehming, 2003; Rice et al., 2003; Hublitz et al., 2009). Furthermore, Ehmt1 is indispensable for mouse embryonic development since homozygous knockout of the gene leads to severe growth retardation and embryonic lethality at E9.5 (Tachibana et al., 2005).

So far, studies investigating Ehmt1 function in vivo have been focused on adaptive behavior and its role in learning and memory, linked to the ID phenotype of KS patients. It was found that knockout of *EHMT* in *Drosophila* led to deficits in non-associative learning and courtship memory (Kramer et al., 2011). Moreover, a conditional knockout of *Ehmt1* in postnatal forebrain revealed deficits in adaptive behavior and associative learning of mice in the fear conditioning paradigm (Schaefer et al., 2009). We examined the *Ehmt1*$^{+/-}$ mice with Ehmt1 haploinsufficiency from development on, and found that these mice display autistic-like features and deficits in learning and memory, together with reduced branching and spine density of hippocampal CA1 neurons and synaptic transmission defects (Balemans et al., 2010, 2013).

The KS phenotype is characterized by (1) moderate to severe developmental delay. This term is used to characterize the developmental status of children under age three, because their cognitive abilities are difficult to assess (Daily et al., 2000). Further KS core features are (2) childhood hypotonia causing feeding difficulties, speech delay, motor delay, and (3) craniofacial abnormalities, including micro- or brachycephaly, hypertelorism, synophrys or arched eyebrows, mid-face hypoplasia, a short nose with upturned nares, a protruding tongue with everted lower lip, upslanted palpebral fissures, down turned corners of the mouth, and prognathism (Stewart and Kleefstra, 2007; Kleefstra et al., 2009; Kleefstra syndrome Leaflet "Unique", 2009; Willemsen et al., 2012). None of these features have yet been assessed in any of the available models.

Mouse models for human diseases are valuable for unraveling molecular mechanisms and pathogenesis, identifying phenotypic features that have gone unnoticed in patients, and developing potential therapeutic interventions. Ideally, the mouse model should be based on a known genetic cause for the disease (construct validity), recapitulate the human phenotypes (face validity), and respond with the same specificity to treatments that are effective in the human disease (predictive validity) (Chadman et al., 2009). In this study we employed *Ehmt1*$^{+/-}$ mice as a model with construct validity, to investigate whether these mice recapitulate developmental features of the KS core phenotype. We show that in addition to ID and autistic-like features (Balemans et al., 2010, 2013), *Ehmt1*$^{+/-}$ mice manifest several developmental defects reminiscent of KS. Moreover, we reveal a possible molecular mechanism for the morphometric skull anomalies by showing that diminished Ehmt1 protein levels and reduced H3K9 dimethylation at bone developmental gene promoter sites, is associated with increased Runx2 and other bone genes mRNA expression in *Ehmt1*$^{+/-}$ mice.

Animals, materials and methods

Animals and genotyping

Male Euchromatin histone methyltransferase heterozygous knockout (*Ehmt1*$^{+/-}$) mice (Tachibana et al., 2005) were bred with female C57BL/6J wildtype mice to obtain wildtype and *Ehmt1*$^{+/-}$ littermates. Mice were genotyped, and housed, as previously described (Balemans et al., 2010). The early postnatal tests were performed before genotyping, thus the entire litter was tested. During testing the mouse pups were identified by marking them with a dye, and at postnatal day (P) 28 a small ear perforation was taken for genotyping and identification during adulthood. All experiments were performed in a blinded fashion.

All procedures involving animals were approved by the Animal Care Committee of the Radboud University Nijmegen Medical Centre, The Netherlands, and conform to the guidelines of the Dutch Council for Animal Care and the European Communities Council Directive 2010/63/EU.

Early postnatal morphological development

Morphological development of the wildtype and *Ehmt1*$^{+/-}$ mouse pups was assessed in three cohorts by three different observers. The weight (g) of the pups was recorded daily from P5 until P25. Furthermore, we recorded the postnatal day at which: (1) nipples were visible in the female pups, (2) the pups had a full grown fur, (3) the lower incisors erupted, (4) the upper incisors erupted, (5) the ears opened and became functional, and (6) the eyes opened. Ear function was assessed by administering an acoustic stimulus and noting the presence/absence of a startle response in the pup. If the two eyes opened at different days, the average was taken.

Early postnatal muscular strength and motor coordination

We used two behavioral tests for muscular strength and motor coordination (van der Meer et al., 1999) in the newly born wildtype and *Ehmt1*$^{+/-}$ mice. The walking test was performed in four cohorts, and the bar holding test in three cohorts by different observers. The mouse pups were scored individually according to four levels each for walking and bar holding. Walking levels were defined as follows: (0) no locomotion; (1) pivoting using head and forelimbs only; (2) crawling with abdomen touching surface; (3) walking on four limbs. Bar holding levels were defined as follows: (0) cannot hold onto bar; (1) holds bar with forepaws only; (2) holds bar with four paws; (3) holds bar with all paws and tail. For both tests, we scored the postnatal day at which the pup reached level 1, 2 or 3. During the bar holding test, we recorded the time (s) the pup was able to hang onto the bar at each postnatal day. During the walking test in the last cohort, we specifically assessed the way of walking. Shaking and unstable walking was noted as 'present' if it occurred at least once between P4 and P11.

Morphometric analysis and inspection of the crania

Wildtype ($n=13$) and *Ehmt1*$^{+/-}$ ($n=12$) female mice of 14 months old were sacrificed, their heads de-skinned and soft tissue removed as much as possible with a scalpel. Crania were further cleaned by placing them for 3 h in 60 °C water containing sodium carbonate (200 g/l). After removing the last remaining tissue, crania were rinsed with water and then air-dried. We measured 10 linear distances with five hundredth of a millimeter accuracy using a vernier caliper. Each distance was measured twice by two independent observers, and these four scores were then averaged. We measured nasal bone length (NL), frontal bone length (FL), parietal bone length (PL), interparietal bone length (IL), nasal bone width (NW), distance between left and right anterolateral corner of the frontal bone (LR), frontal bone width (FW), and interparietal bone width (IW), as adopted from (Kawakami and Yamamura, 2008). Total cranial length (TL, measured as the distance between the upper incisors and the occipital bone) and parietal bone width (PW) were recorded as well. Complete or incomplete fusion of the left and right frontal bones was assessed by visual inspection, with the crania placed on a light box with light coming from

Table 1
Number of adult wildtype and *Ehmt1*$^{+/-}$ mice without or with a bent nose.

	Straight Nose	**Bent Nose**	*Age in months*
	(*n*)	(*n*)	(*n straight nose*)
Male wildtype	14	0	*1mo* (*8*), *3mo*(*6*)
Female wildtype	35	0	*1mo* (*10*), *3mo* (*5*), *6mo* (*7*), *14mo* (*13*)
Total wildtype	**49**	**0**	
	(n)	(n)	(*n Straight nose*; *n bent nose*)
Male *Ehmt1*$^{+/-}$	12	9	*1mo*(*5*;*4*), *3mo*(*1*;*2*), *6mo*(*0*;*1*), *16mo*(*3*;*1*), *23mo*(*3*;*1*)
Female *Ehmt1*$^{+/-}$	21	9	*1mo*(*6*;*1*), *3mo*(*4*;*2*), *6mo*(*3*;*2*), *14mo*(*8*;*4*)
Total *Ehmt1*$^{+/-}$	**33**	**18***	

Skulls of adult mice with ages ranging from 1 to 23 months old were analyzed for the absence or presence of a "bent nose", which was characterized by a deviation of $\geq 15^{\circ}$ from the nose bones midline. This table includes the 13 wildtype and 12 *Ehmt1*$^{+/-}$ mice (14 months of age) used for the morphological skull measurements.

* Significantly different from wildtype (Chi-square test $p < 0.001$).

underneath. The absence or presence of a bent nose, characterized by $\geq 15^{\circ}$ deviation from the midline, was assessed at the time of dissection in postnatal P2, P4, P8, P14 mice ($n=5$ per age, per genotype), and in adult wildtype ($n=49$) and *Ehmt1*$^{+/-}$ ($n=51$) mice at the age of 1, 3, 6, 14, 16 or 23 months (Table 1).

Preparation of histological sections and haematoxylin/eosin (HE) staining

Mice were sacrificed by cervical dislocation at the age of 5 days, 1 mo or 3 mo. P5 whole heads were frozen in liquid nitrogen, stored at −80 °C, and sagittal 10 μm sections could be cut on the cryostat without previous decalcification. For the adult mice, the head was de-skinned and the entire skull cleaned off soft tissue. The P28 skulls, containing the parietal and frontal bones, were dissected and fixed in 4% paraformaldehyde, decalcified in 10% EDTA for 2 days, embedded in paraffin and cut coronally at 7 μm thickness. The two nose bone pieces were taken from the skull of the 3 mo old mice and decalcified in 10% EDTA for 2 days. Using Shandon M-1 embedding matrix (Thermo Scientific) and a cryostat at −20 °C, horizontally oriented nose bone pieces were cut at 10 μm thickness and captured on Superfrost Plus slides (Thermo Scientific).

P5 head and adult skull and nose bone sections were stained with haematoxylin for 10–20 min, rinsed with running tap water for 7 min, dipped in 50% ethanol, and stained with eosin for 1–2 min. Sections were then dehydrated with increasing ethanol concentrations, cleared in xylene, and mounted with Pertex (Histolab Products AB, Göteborg, Sweden).

Westen blot analysis and immunocytochemistry

Western blot analysis for Ehmt1 protein was performed on P28 brain tissue of wildtype and *Ehmt1*$^{+/-}$ mice, as previously described (Balemans et al., 2013).

Ehmt1 immunostaining

Sections were fixed and permeabilized with ice-cold methanol for 10 min at −20 °C and washed four times with TBS-T (50 mM Tris–HCl pH 7.5, 150 mM NaCl, 0.05% Tween-20). Immunocytochemical staining was performed according to the UltraTek HRP Anti-Polyvalent Staining System from ScyTek (ScyTek Laboratories, Inc.). Briefly, sections were incubated with Super Block for 5 min, followed by a short wash with TBS-T, and overnight incubation with mouse-anti-Ehmt1 antibody (1:200, ab41969, Abcam) in blocking buffer (1% bovine serum albumin, 1% glycine in TBS-T) at 4 °C. After four 10 min washes with TBS-T, the sections were incubated for 10 min with UltraTek Anti-Polyvalent, washed four times with TBS-T, and incubated for 10 min with UltraTek HRP. Three TBS-T washes were followed by two TB washes (50 mM Tris–HCl pH 7.5) and a 10 min incubation with 3,3′-diaminobenzidine (DAB). The DAB reaction was stopped by three more washes with TB. Sections were then dehydrated with increasing ethanol concentrations, cleared in xylene, and coverslipped with Pertex (Histolab Products AB, Göteborg, Sweden).

Osteopontin immunostaining

Sections were fixed and permeabilized with ice-cold methanol for 10 min at −20 °C, washed four times 5 min with PBS-T (0.1 M PBS, 0.1% Tween-20), and incubated with blocking buffer (1% bovine serum albumin, 1% glycine in PBS-T) for 30 min. Rabbit anti-osteopontin (1:1000, Sigma) in blocking buffer was then applied and incubated overnight at 4 °C. After a three times 5 min rinse in PBS-T, the sections were incubated with a donkey-anti-rabbit biotinylated secondary antibody (1:250, Jackson ImmunoResearch Laboratories) in blocking buffer for 1 h, followed by three times 5 min wash in PBS-T. The avidin–biotin complex solution (1:125; ABC Vectastain Elite, Sigma) in PBS was made 30 min prior to use, sections were incubated for 30 min, and rinsed three times 5 min in PBS. Finally, the slides were placed into the 3-amino-9-ethylcarbazole (AEC) substrate solution (0.02% AEC in *N*,*N*-dimethylformamide and 0.01% H_2O_2 in 35 mM NaAc-HAc, pH 4.9) for 10 min. The reaction was stopped by rinsing with distilled water. Sections were coverslipped using Kaiser′s gelatin–glycerol.

Runx2 immunostaining

The fixed and paraffin skull bone sections were de-paraffinized, washed with PBS (0.1 M PBS), incubated with blocking buffer for 1 h (5% rabbit serum, 5% fetal calf serum, 0.1% Triton X-100), and incubated with primary antibody goat anti-Runx2 (1:80, Sigma) in blocking buffer overnight at 4 °C. After three times 5 min wash in PBS, the sections were incubated with a rabbit-anti-goat biotinylated secondary antibody (1:250, Jackson ImmunoResearch Laboratories) in blocking buffer for 30 min, followed by three times 5 min wash in PBS. The avidin–biotin complex solution (1:125; ABC Vectastain Elite, Sigma) in PBS was made 30 min prior to use, sections were incubated for 30 min, and rinsed three times 5 min in PBS. Finally, DAB substrate solution (with 10 μl H_2O_2) was added for 10 min, after which the reaction was stopped by rinsing with distilled water. Sections were dehydrated and coverslipped. Using Fiji (Image J) software, Runx2 immunostaining density was measured for 60 osteoblasts and 60 osteocytes in wildtype and *Ehmt1*$^{+/-}$ skull sections, positioned adjacent on one glass slide. The density values (range 0–256) have been reversed by subtracting from 256, with dark osteoblasts at ~115–122 and lighter osteocytes at ~70–80.

RNA isolation

For expression analysis in brain tissue, both hippocampi of P28 wildtype ($n=4$) and *Ehmt1*$^{+/-}$ mice ($n=4$) were quickly dissected, frozen in liquid nitrogen and stored at −80 °C. RNA was isolated using the NucleoSpin RNA II (Clontech, 740955) kit according to the manufacturer′s protocol. cDNA was synthesized from 1.0 μg total RNA using SuperScript II reverse transcriptase (Invitrogen), and stored at −20 °C.

For expression studies in bone tissue, the parietal and frontal skull bones were dissected from P28 (wildtype $n=9$, *Ehmt1*$^{+/-}$ $n=9$) and P8 (wildtype $n=7$, *Ehmt1*$^{+/-}$ $n=3$) mouse crania. After thorough removal of all soft tissue using a scalpel knife, the cleaned skull bones were snap frozen in liquid nitrogen and stored at −80 °C. Frozen bone tissue was crushed in a dismembrator capsule, containing a ball,

chilled with liquid nitrogen, at 1500 rpm for 1 min. RNA was extracted using the RNeasy Mini Kit for fibrous tissue (Qiagen, Inc., Valencia, CA, USA, nr 74704), treated with DNAse1 (Invitrogen), and reverse transcribed using M-MLV RT with oligo(dT) primers (Invitrogen) to produce cDNA, stored at −20 °C.

Quantitative real-time PCR analysis

Quantitative PCR primers were designed using Primer3 (http://www.frodo.wi.mit.edu; for list of primers used see Supplemental Table S1), and qPCR reactions were performed in the 7500 Fast Real Time PCR System apparatus (Applied Biosystems) by using iQ SYBR Green Supermix (Biorad) according to the manufacturer's protocol. Relative mRNA expression levels for Runx2, Col22a1, Col11a1, and Dmp1 were calculated using the $2^{\Delta\Delta Ct}$ method (Livak and Schmittgen, 2001) with standardization to Srp9 (Signal recognition particle 9) expression levels. The difference in mRNA expression of each gene between wildtype and *Ehmt1*$^{+/-}$ mouse tissue samples is depicted as fold increase (f.i., 1.4x for Runx2) with wildtype relative mRNA levels set at 1.

H3K9me2 chromatin immunoprecipitation (ChIP)

The hippocampi of three P28 wildtype and three P28 *Ehmt1*$^{+/-}$ mice were quickly dissected and pooled (to obtain sufficient amounts of DNA) per genotype, and subsequently treated with 1% formaldehyde to crosslink chromatin followed by tissue homogenization in PBS. The crosslinked chromatin was fragmented by sonicating three times for eight minutes at high power for 30 s on/off with a Bioruptor (Diagenode). Chromatin immunoprecipitation (ChIP) was performed as described (Kramer et al., 2011), to capture antibody-bound chromatin by using anti-H3K9me2 antibody (07–441, Upstate) and Prot A/G beads (Santa Cruz). The enriched ChIPed DNA was quantified by Qubit fluorometer, using the Quant-iT dsDNA HS Assay Kit (Invitrogen, Q32851) and analyzed by subsequent quantitative real-time PCR (qPCR) reactions. To perform qPCR, various primers were designed (using Primer3; for list of primers used see Supplemental Table S1) around the promoter of genes from 0.5 kb upstream to 1.0 kb downstream of the transcription start site at an interval of about 250 bp.

For analysis the −0.5 to +1.0 kb region around the transcriptional start sites was targeted as previous studies have revealed that this region encompasses H3K9me2 profiles controlled by Ehmt (Barski et al., 2007; Marks et al., 2009; Kramer et al., 2011). The β-actin promoter region was used here as a reference.

Statistical analyses

All data are presented as means ± SEM. The statistical significance of differences between groups was assessed using the independent samples *t*-test, ANOVA repeated measures test, or Chi-square test. All statistical procedures were performed using the SPSS 17.0 and 20.0 software packages. Statistical significance was set at $p < 0.05$.

Results

Ehmt1$^{+/-}$ *mouse pups demonstrate delayed postnatal development*

KS patients are characterized by developmental delay (Daily et al., 2000;Iwakoshi et al., 2004;Stewart and Kleefstra, 2007).

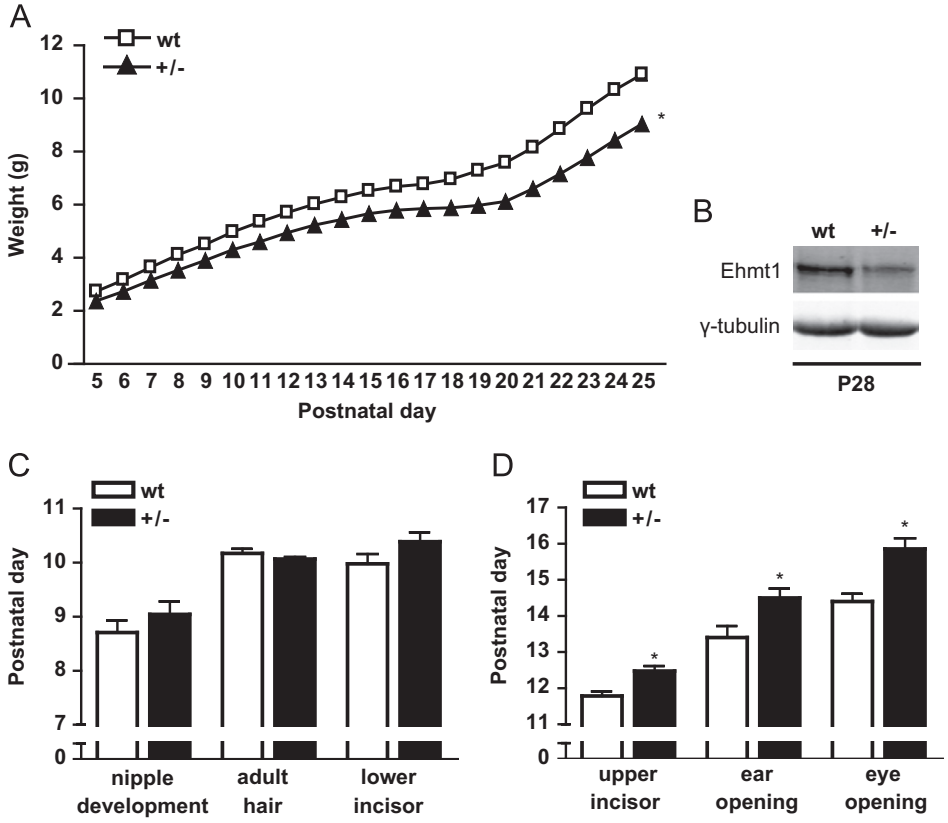

Fig. 1. Postnatal developmental delay in *Ehmt1*$^{+/-}$ mice. Wildtype ($n=52$) and *Ehmt1*$^{+/-}$ ($n=52$) pups were weighed daily from postnatal day 5–25, with *Ehmt1*$^{+/-}$ pups showing a significantly lower weight at each postnatal day (A). Compared with wildtypes, the *Ehmt1*$^{+/-}$ mice showed a 50% reduction of Ehmt1 protein levels in P28 brain tissue, with γ-tubulin used as a loading control (B). Nipple development was comparable between wildtype ($n=17$) and *Ehmt1*$^{+/-}$ ($n=23$) female pups. Also the day the pups had a full grown fur, and the lower incisors erupted were equal for both genotypes (wildtype $n=42$ and *Ehmt1*$^{+/-}$ $n=44$; C). At later developmental stages, we observed significantly delayed upper incisor eruption, ear opening, and eye opening in *Ehmt1*$^{+/-}$ ($n=44$) pups compared with wildtype ($n=42$; D). *=significantly different from wildtype.

We assessed postnatal development in wildtype and *Ehmt1*$^{+/-}$ mouse pups. Body weight was measured daily from postnatal day P5 until P25. Both genotypes gained weight over time, but the body weight of *Ehmt1*$^{+/-}$ mice was significantly reduced at every postnatal day when compared with wildtypes (Fig. 1A, *t*-tests for every single timepoint: $p<0.001$; ANOVA repeated measures, genotype × age: $F_{1,102}=39.621$, $p<0.001$). When *Ehmt1*$^{+/-}$ mice reach adulthood, however, the average body weight is similar to that in wildtypes (Balemans et al., 2010, 2013), indicating that the observed reduction in body weight is specific for neonatal development. This is in accordance with the recently reported high Ehmt1 protein levels at postnatal day 4, which declined to 50% at P8, to 25% at P14, and to 10% of the P4 level by the time the animals were 1 month old (Balemans et al., 2013). Compared with wildtype, the *Ehmt1*$^{+/-}$ mice demonstrated ~50% Ehmt1 protein reduction at all times analyzed and is shown here for P28 brain tissue (Fig. 1B).

During the first two postnatal weeks, mice develop a fur, lower and upper incisors appear, the ears and eyes open, and females develop nipples. When assessing these parameters in *Ehmt1*$^{+/-}$ mice, we noted that the earlier developmental changes (nipple development, fur formation, and lower incisor eruption) were similar between the genotypes (Fig. 1C). At later postnatal days, however, *Ehmt1*$^{+/-}$ pups showed a significantly delayed onset of 1 to 2 days of upper incisor eruption ($p<0.001$), ear opening ($p<0.009$), and eye opening ($p<0.001$), compared with wildtype (Fig. 1D). These data indicate delayed postnatal development in *Ehmt1*$^{+/-}$ pups.

Ehmt1$^{+/-}$ *mouse pups show hypotonia*

Another core feature of KS is childhood hypotonia. To assess this in the *Ehmt1*$^{+/-}$ mice we performed two tests for muscular function. Walking behavior was studied from P4 until P11 according to three different levels of maturity. At P4 all pups had already reached walking level 1. Interestingly, *Ehmt1*$^{+/-}$ pups reached both walking level 2 and 3 almost one full day later than wildtype pups ($p<0.008$ and $p<0.006$ respectively, Fig. 2A). In a part of the cohort, we closely assessed the way of walking, which revealed a significantly higher percentage of *Ehmt1*$^{+/-}$ mice displaying a shaking and unstable way of walking ($\chi^2_1=7.738$, $p<0.005$, Fig. 2B).

Bar holding ability was tested from P11 until P19. Compared with wildtype, *Ehmt1*$^{+/-}$ pups reached each level of bar holding almost half a day later, although this only reached significance for level 1 ($p<0.007$, Fig. 2C). The amount of time the pups were able to hang on to the bar was also measured. Bar holding time increased over days for both genotypes, however *Ehmt1*$^{+/-}$ pups showed significantly decreased bar holding times compared with their wildtype littermates ($F_{1,68}=11.980$, $p<0.001$, Fig. 2D). Together, these data show early postnatal hypotonia and motor function delay in *Ehmt1*$^{+/-}$ mouse pups.

Ehmt1$^{+/-}$ *mice have cranial abnormalities*

Cranial and facial characteristics are important determinants for the clinical diagnosis of KS. To determine whether the *Ehmt1*$^{+/-}$ mice have similar morphological anomalies, the lengths and the widths of the different cranial parts were measured (Fig. 3A and B). The length of the entire skull, and the nasal bone, frontal bone and parietal bone length were significantly shorter in 12 *Ehmt1*$^{+/-}$ mice when compared with 13 wildtypes (TL: $p<0.001$, NL: $p<0.03$, FL: $p<0.009$, PL: $p<0.0001$; Fig. 3A). The width of the occipital bone was smaller (IW: $p<0.006$), whereas the width of the frontal bone and between its anterolateral corners was significantly wider in *Ehmt1*$^{+/-}$ mice (FW: $p<0.02$; LR: $p<0.0001$, Fig. 3A and B). When taking into account the shorter and wider crania (defined as brachycephaly), the shorter nasal bone length, and the wider LR distance (which causes the eyes to

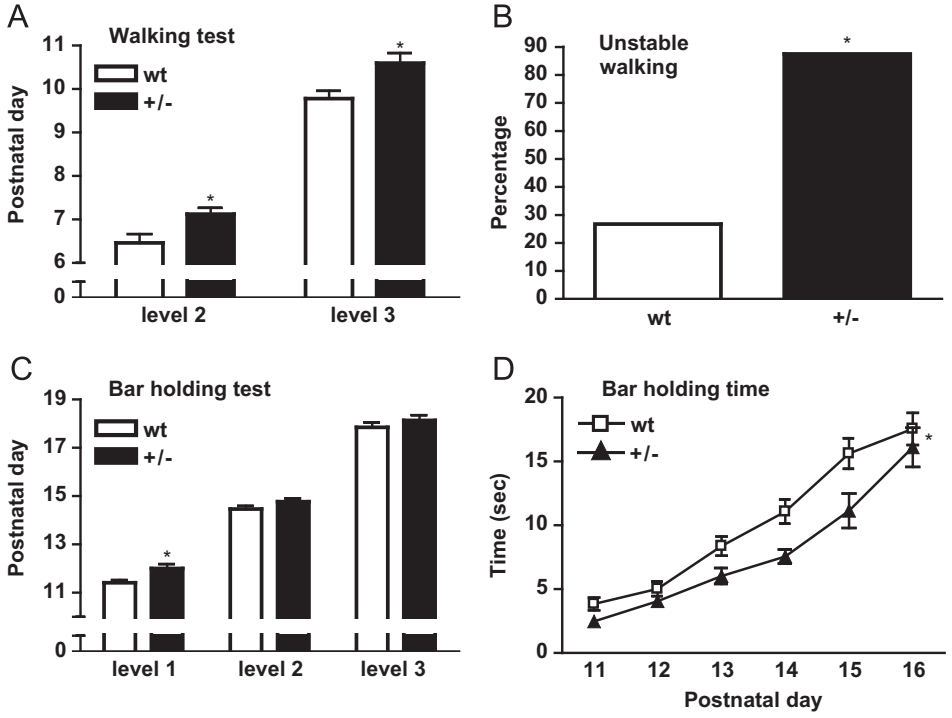

Fig. 2. Hypotonia in newborn Ehmt1$^{+/-}$ mice. *Ehmt1*$^{+/-}$ ($n=52$) pups reached both level 2 and level 3 of walking significantly later compared with wildtype ($n=52$; A). Shaking/unstable walking was noted when it occurred at least once between postnatal day 4 and 11, this was significantly more often observed in *Ehmt1*$^{+/-}$ ($n=8$) compared with wildtype pups ($n=15$; B). Wildtype ($n=39$) and *Ehmt1*$^{+/-}$ ($n=37$) pups were observed daily for the day at which they reached level 1, 2 and 3 of bar holding (C). *Ehmt1*$^{+/-}$ ($n=37$) pups hung on to the bar significantly shorter compared with wildtype littermates ($n=39$; D). *=significantly different from wildtype.

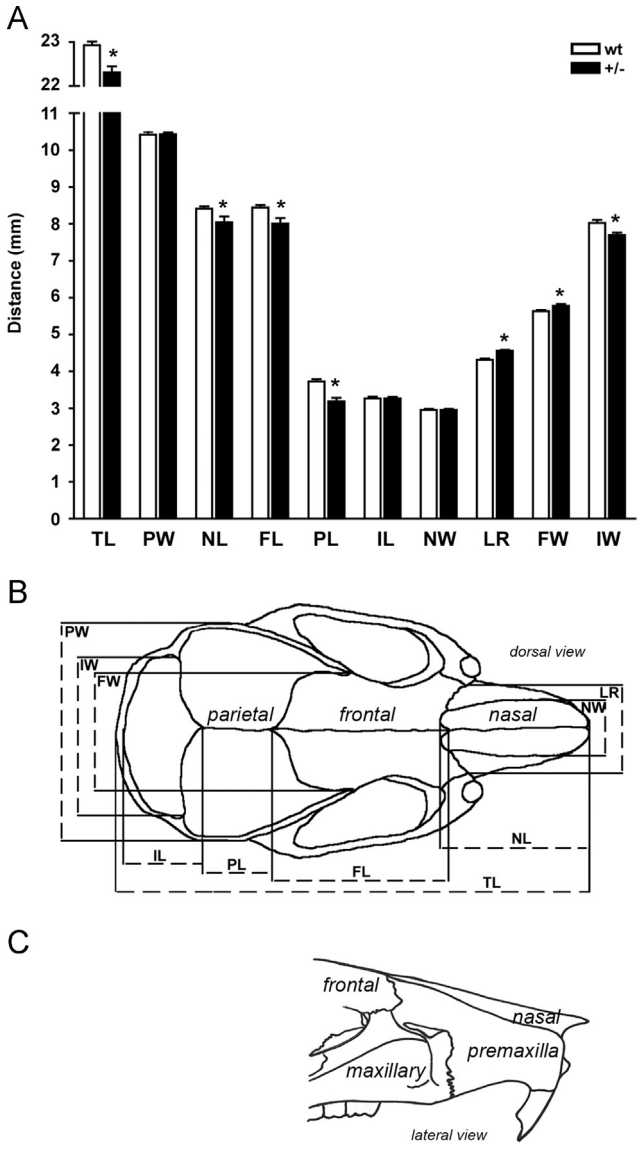

Fig. 3. Morphometric analysis of wildtype and *Ehmt1*$^{+/-}$ crania. (A) For each of the wildtype ($n=13$) and *Ehmt1*$^{+/-}$ ($n=12$) crania, 10 linear cranial distances are plotted here with five hundredth of a millimeter accuracy. *=significantly different from wildtype. (B) Drawing dorsal view of a mouse skull, indicating TL total length, PW parietal bone width, NL nasal bone length, FL frontal bone length, PL parietal bone length, IL interparietal bone length, NW nasal bone width, LR distance between left and right anterolateral corner of frontal bone, FW frontal bone width, IW interparietal bone width. (C) Drawing lateral view of a mouse skull with suture between maxillary and premaxilla bones.

be further apart, defined as hypertelorism), these data imply that *Ehmt1*$^{+/-}$ mice indeed show cranial abnormalities that correspond to those seen in KS patients.

Upon examination of the morphology of the 14 mo old mouse crania it was noted that 4 of the 12 *Ehmt1*$^{+/-}$ crania had a bent nose, whereas none of the 13 wildtype crania showed this (Chi-square test $\chi^2_1=5.159$, $p<0.023$, Fig. 4, Table 1). To confirm this observation, we assessed the absence or presence of the bent nose phenotype in a larger group of mice at different ages and of different generations. At the postnatal age of P2, P4, P8 or P14 ($n=5$ per age, genotype) skull observations revealed no bent nose in wildtypes or *Ehmt1*$^{+/-}$ mice. However, 35% of the 51 adult *Ehmt1*$^{+/-}$ mice showed a bent-nose phenotype compared with none of the 49 adult wildtypes (Chi-square $\chi^2_1=21.090$, $p<0.001$; Table 1). This accounted for the adult age range of 1–23 months. For the 18 bent noses (Table 1), deviation of snout direction occurred equally to the left or to the right.

In addition, one of the *Ehmt1*$^{+/-}$ crania showed a large hole along the midline which meant an incomplete fusion of the left and right frontal bones (see Fig. 3B, and arrow in Fig. 4D). More detailed investigation revealed a small hole between the frontal bones (posterior region) in 2 of the 13 wildtype and 9 of the 12 *Ehmt1*$^{+/-}$ mice. Concluding, significantly more *Ehmt1*$^{+/-}$ mice showed incomplete posterior frontal suture fusion compared with wildtype animals (Chi-square $\chi^2_1=9.000$, $p<0.003$; Fig. 4). Lateral view examination of the left and right snout parts of the 25 skulls revealed a normal, interdigitated, premaxillary suture (Fig. 3C) between the maxillary bone and premaxilla bone, in both genotypes (not shown).

Ehmt1 protein is present in postnatal and adult osteocytes and osteoblasts

The bent-nose phenotype like in the *Ehmt1*$^{+/-}$ mice has also been observed in other mouse models, including the Apert syndrome *Fgfr2* mutant mouse and Saethre-Chotzen syndrome *twist*-null mouse (Bourgeois et al., 1998;Yin et al., 2008). Therefore, we hypothesized that the distorted crania in *Ehmt1*$^{+/-}$ mice could be caused by aberrant expression of bone tissue related genes.

For this, it was investigated whether the Ehmt1 protein was present in bone cells. The osteopontin bone tissue marker revealed the location of osteoblasts and osteocytes in P5 wildtype and *Ehmt1*$^{+/-}$ cranial bone tissue (Fig. 5A and B). Haematoxylin and eosin (HE) staining of P5 mouse head showed developing bone with surrounding connective tissue, striated muscle cells and hair follicles (Fig. 5C and F). Using anti-Ehmt1 immunostaining it was demonstrated that Ehmt1 protein was indeed present in osteoblasts and osteocytes of P5 wildtype and *Ehmt1*$^{+/-}$ cranial tissue (Fig. 5D and E). Furthermore, nose bone pieces from 3 months old wildtype and *Ehmt1*$^{+/-}$ mice contained osteocytes, as shown by osteopontin and HE staining (Fig. 5G and I). Osteocytes and osteoblasts in 3 months old nose bone tissue clearly contained Ehmt1 protein, both in wildtype and *Ehmt1*$^{+/-}$ mice (Fig. 5J and K). Of note, no immunoreactivity was observed when the primary antibody for Ehmt1 was omitted (Fig. 5L). Lastly, Ehmt1 protein expression was observed in P5 striated muscle cells (Fig. 5M), odontoblasts of the developing tooth (Fig. 5N), and retinal cell layers (Fig. 5O), the development of which were all delayed in *Ehmt1*$^{+/-}$ mice (Figs. 1 and 2).

Ehmt1$^{+/-}$ *mice demonstrate increased expression of bone tissue related genes*

Next, it was investigated whether the reported reduced Ehmt1 protein levels in *Ehmt1*$^{+/-}$ mice (Balemans et al., 2013; Fig. 1B,) could affect the expression of bone tissue related genes, due to decreased histone H3 lysine 9 dimethylation (H3K9me2) levels. Notably, H3K9me2 is an epigenetic mark for transcriptional silencing (Hublitz et al., 2009) and Tachibana et al. (2005) reported diminished H3K9me2 in *Ehmt1*$^{+/-}$ stem cells. An RNA-sequencing dataset comparing P28 wildtype and *Ehmt1*$^{+/-}$ hippocampal brain tissue (personal communication from co-authors M. Ansar and H. Zhou) revealed that from all the ($\geq 1.4\times$) upregulated genes, four genes were related to bone tissue development. Performing quantitative PCR experiments confirmed the increased mRNA levels for the four bone genes in brain tissue of *Ehmt1*$^{+/-}$ mice when compared with wildtypes (Fig. 6A, B, C and D and D; $n=4$ per genotype). *Runx2* mRNA levels were 1.4 times increased ($p<0.027$), *Col22a1* levels were 2.9 fold higher ($p<0.01$), *Col11a1* showed a 1.5 fold increase in mRNA levels ($p<0.075$), and *Dmp1* levels were 1.7 times higher ($p<0.001$) in *Ehmt1*$^{+/-}$ tissue

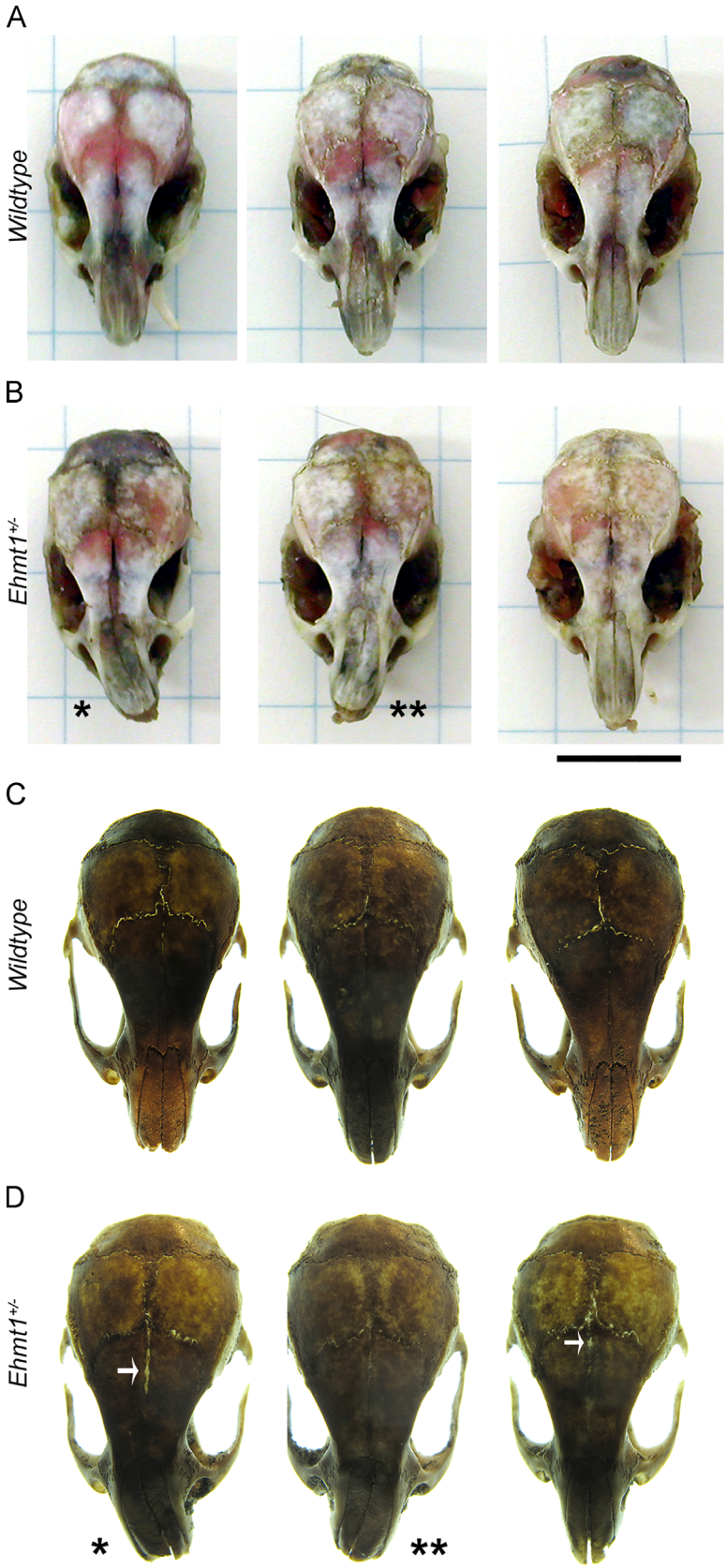

Fig. 4. Morphology of wildtype and *Ehmt1*$^{+/-}$ crania. Photographs of three representative wildtype (A and C) and *Ehmt1*$^{+/-}$ (B and D) crania, taken with light from above (A and B) or from underneath to visualize suture openings and holes (C and D). One third of the *Ehmt1*$^{+/-}$ mice showed a bent nose phenotype, which could be to the left (*) or to the right (**). Bar in B (for A and B) is 1 cm. The arrows in D indicate incomplete fusion of the left and right frontal bones, which was observed in the majority of the *Ehmt1*$^{+/-}$ crania.

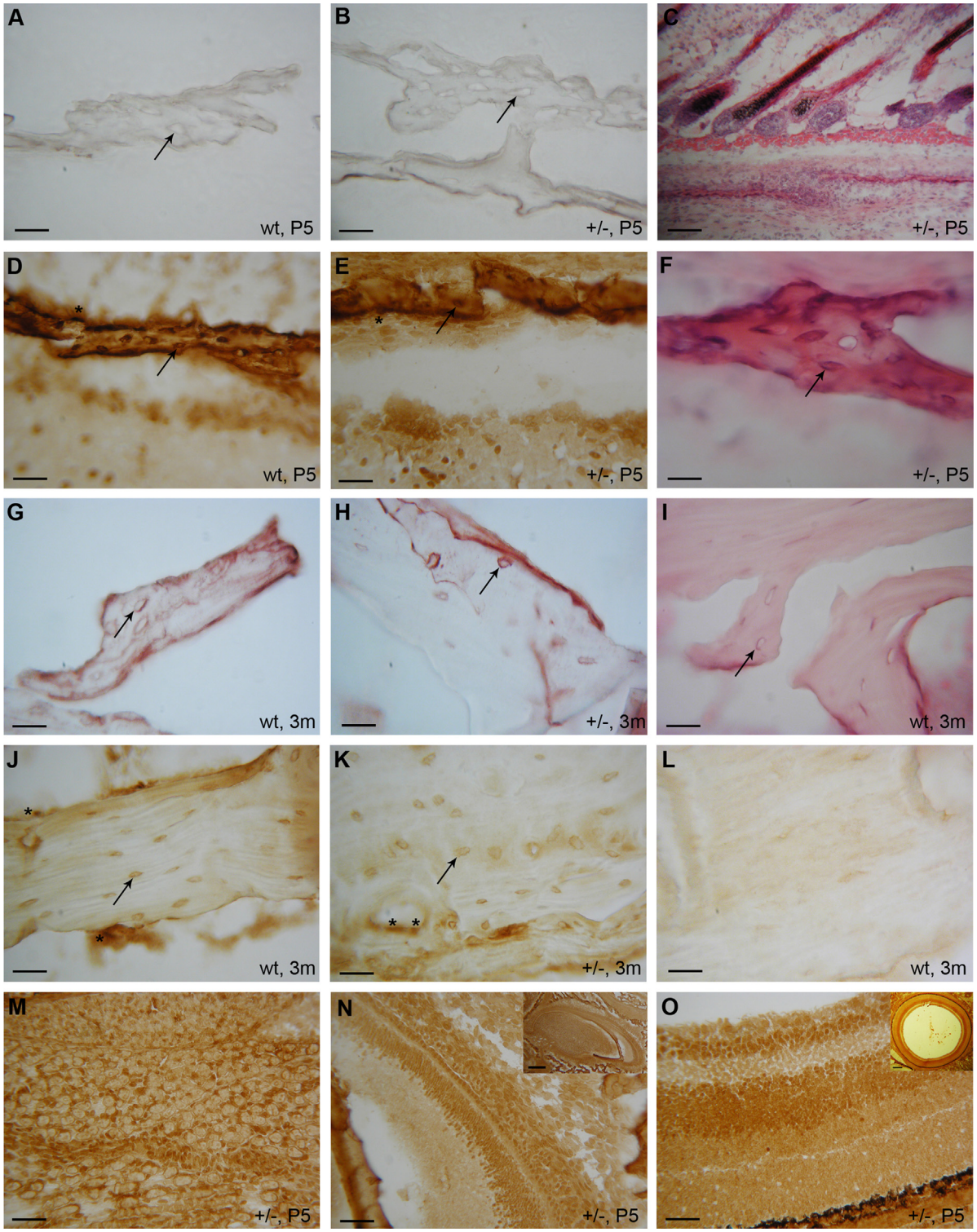

Fig. 5. Ehmt1 protein expression in osteoblasts and osteocytes. Immunostaining for osteopontin (A, B, G and H) revealed the presence of osteoblasts and osteocytes in postnatal day 5 (P5) cranial bone tissue of wildtype (A) and *Ehmt1*$^{+/-}$ (B) mice, and nose bone of 3 months old wildtype (G) and *Ehmt1*$^{+/-}$ (H) mice. Haematoxylin and eosin (HE) histochemical staining visualized skull structures at P5 as shown with low (C) and high (F) magnification, and morphology of 3 months old nose bone (I) in wildtype and *Ehmt1*$^{+/-}$ mice. Immunostaining for Ehmt1 (D, E, J and K) indicated the presence of Ehmt1 protein in osteoblasts and osteocytes in cranial bone tissue of wildtype (D) and *Ehmt1*$^{+/-}$ (E) P5 mice, and in nose bone of 3 months old wildtype (J) and *Ehmt1*$^{+/-}$ (K) mice. Note the absence of immunoreactivity (L), when the primary antibody for Ehmt1 was omitted. The Ehmt1 protein was also present in skeletal muscle (M), incisor tooth (N, and inset overview) and in eye retinal cells (O, and inset overview) of P5 wildtype and *Ehmt1*$^{+/-}$ mice. The arrows point at the osteocytes, the asterisks (*) indicate the location of osteoblasts. Bar in A, B, F, G, H, I=20 μm; bar in C=80 μm; bar in D, E, J, K, L=32 μm; bar in M, N, O=50 μm.

(Fig. 6A B, C and D). Of note, no alterations were observed in mRNA levels of *Fgfr2* and *Twist1,* the two genes for which mutant alleles give rise to a bent-nose phenotype in mice (data not shown).

Subsequently, the mRNA levels of the first four mentioned bone genes were assessed in parietal and frontal skull bone tissue of P8 and P28 wildtype and *Ehmt1*$^{+/-}$ mice (Fig. 6E, F, G and H).

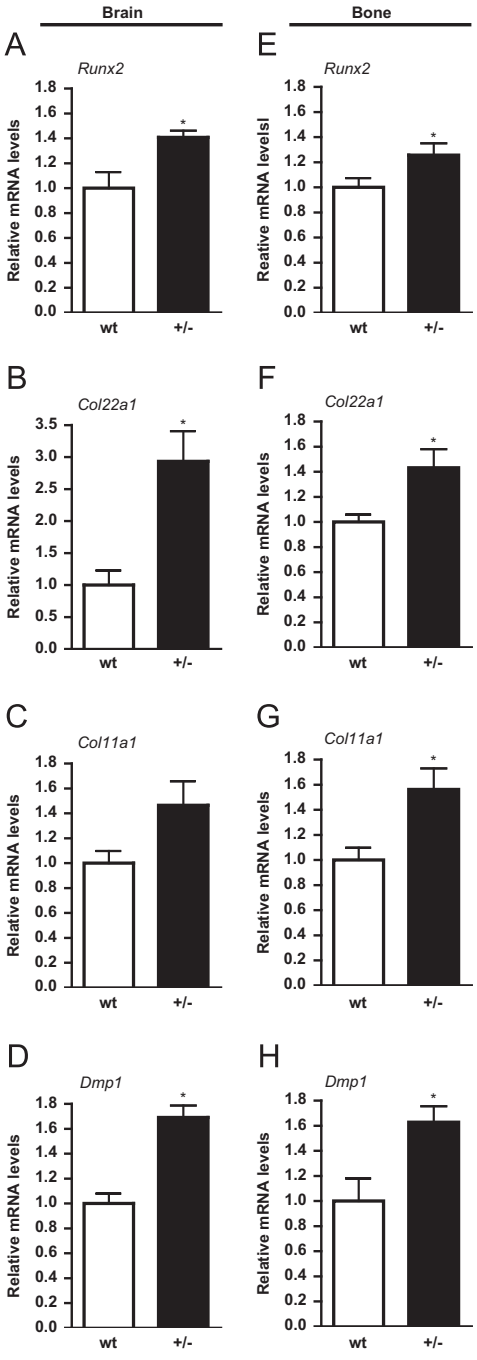

Fig. 6. Increased expression of bone tissue related genes in *Ehmt1*$^{+/-}$ mice. Quantitative PCR analysis of P28 hippocampal brain tissue from *Ehmt1*$^{+/-}$ mice ($^{+/-}$, $n=4$) demonstrated increased mRNA expression for *Runx2* (A), *Col22a1* (B), *Col11a1* (C), and *Dmp1* (D) compared with wildtype mice (wt, $n=4$). The qPCR analysis of P28 skull bone from *Ehmt1*$^{+/-}$ mice ($n=9$) showed significantly increased mRNA expression of the bone tissue related genes *Runx2* (E), *Col22a1* (F), *Col11a1* (G), and *Dmp1* (H) compared with wildtype mice ($n=9$). (For *Dmp1*, values are the average of $n=4$ wildtype and $n=6$ *Ehmt1*$^{+/-}$ mice.) *Indicates significantly different from wildtype.

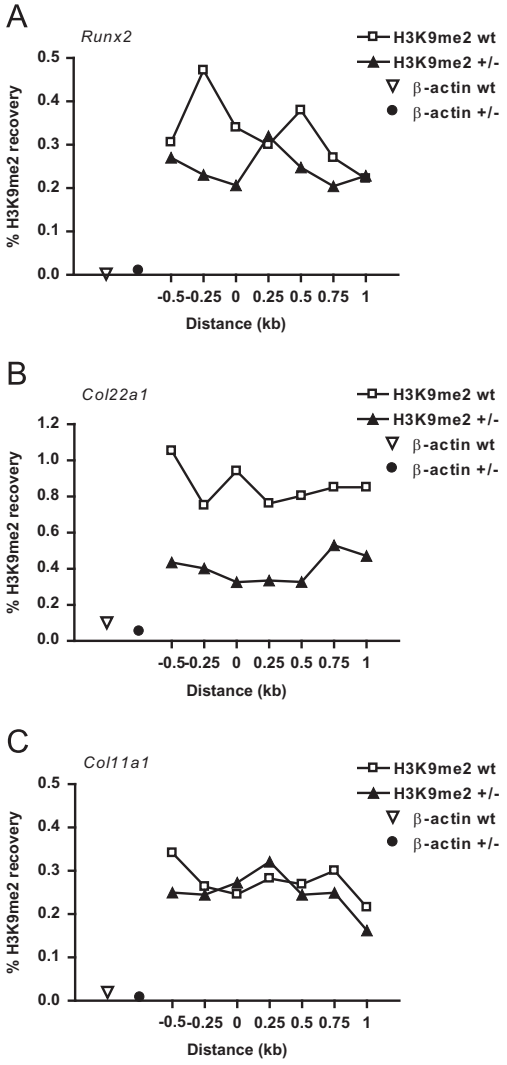

Fig. 7. Decreased H3K9 dimethylation of bone gene promoter sites in *Ehmt1*$^{+/-}$ mice. The extent of histone H3 Lysine 9 dimethylation (H3K9me2) in *Ehmt1*$^{+/-}$ mouse brain tissue, examined at the -0.5 to $+1.0$ kb region around the transcriptional start site of the *Runx2*, *Col22a1* and *Col11a1* genes, demonstrated a strong reduction in % H3K9me2 recovery levels for *Runx2* (A) and *Col22a1* (B), and less pronounced for *Col11a1* (C), when compared with wildtypes. The β-actin promoter region was used as a reference, with low % H3K9me2 recovery levels (A)–(C).

Quantitative PCR analysis demonstrated similar significant increases in mRNA levels of *Runx2* ($p<0.05$), *Col22a1* ($p<0.015$), *Col11a1* ($p<0.01$), and *Dmp1* ($p<0.019$) in P28 *Ehmt1*$^{+/-}$ skull bone tissue compared with wildtype skull (Fig. 6E, F, G and H; $n=9$ per genotype). Thus, gene expression of the four mentioned genes involved in bone morphogenesis was significantly increased both in brain and in skull bone of *Ehmt1*$^{+/-}$ mice. No significant differences in mRNA levels were observed between skull bone tissue of P8 wildtype ($n=7$) and P8 *Ehmt1*$^{+/-}$ ($n=3$) mice (data not shown).

Increased mRNA levels are associated with diminished H3K9 dimethylation in Ehmt1$^{+/-}$ *mice*

We then examined whether the enhanced mRNA expression was correlated with the alteration of H3K9me2 levels. Chromatin-immunoprecipitation was used to determine the genomic occupancy of H3K9me2 at around the transcription start sites of *Runx2*, *Col22a1*, *Col11a1* and *Dmp1*, and performed in readily available brain tissue of P28 wildtype and *Ehmt1*$^{+/-}$ mice. The analysis was targeted to the -0.5 to $+1.0$ kb region of the transcriptional start sites, as previous studies have revealed that this region encompasses H3K9me2 profiles controlled by Ehmt (Barski et al., 2007; Marks et al., 2009; Kramer et al., 2011). A strong reduction in H3K9me2 levels was apparent at the *Runx2* and *Col22a1* transcriptional start sites in *Ehmt1*$^{+/-}$ mice compared with wildtype (Fig. 7A and B). This reduction of H3K9me2

was less pronounced for *Col11a1* (Fig. 7C). For *Dmp1*, no changes in H3K9me2 levels were observed between the genotype groups (data not shown). The β-actin promoter region was used as a reference gene, with low % H3K9me2 recovery levels (Fig. 7A, B and C). Together, this suggests that the enhanced mRNA levels of the bone tissue related genes, like *Runx2*, *Col22a1* and *Col11a1,* resulted from the decreased H3K9me2 levels in *Ehmt1*$^{+/-}$ mice.

Runx2 immunostaining in P28 skull bone of wildtype and Ehmt1$^{+/-}$ *mice*

To investigate whether increased *Runx2* mRNA would result in higher Runx2 protein expression in P28 skull tissue, the presence of Runx2 protein in bone cells from P28 wildtype and Ehmt1$^{+/-}$ mice was observed in coronal 7 μm thin paraffin frontal skull bone sections.

Haematoxylin and eosin (HE) histochemical staining visualized the characteristic double plate structure of skull bone, with the osteocytes in the bone matrix and osteoblasts in the space between the plates, in P28 wildtype and *Ehmt1*$^{+/-}$ mice (Fig. 8A and B). Immunostaining for Runx2 (Fig. 8C, D, E, F, G, H, I) indicated the presence of Runx2 protein in osteoblasts and osteocytes in skull bone tissue of P28 wildtype (Fig. 8C, E, G and I) and *Ehmt1*$^{+/-}$ (Fig. 8D, F, H and J) mice. Shown are lateral (Fig. 8C and D) and more central (Fig. 8E and F) portions of the coronal skull sections. Note the dark Runx2 immunostaining density of the aligning osteoblasts in the enlarged photographs for wildtype and *Ehmt1*$^{+/-}$ (Fig. 8G and H). Osteocytes contained a lighter Runx2 density as shown for wildtype and *Ehmt1*$^{+/-}$ (Fig. 8I and J). Quantification of Runx2 immunostaining density demonstrated significantly higher values for *Ehmt1*$^{+/-}$ osteoblasts (5% increase, $^{*}p < 0.005$) and osteocytes (12% increase, $^{**}p < 0.001$), compared to wildtype density values (Fig. 8K). Ectopic bone/cartilage was observed underneath the P28 *Ehmt1*$^{+/-}$ skull stained for HE (Fig. 8L), and shown at higher magnification with Runx2 immunostaining (Fig. 8M), revealing an exaggerated Runx2 immunoreactivity in the cells.

Discussion

In this study we show that *Ehmt1*$^{+/-}$ mice recapitulate the developmental delay, hypotonia, and cranial abnormalities, which are three of the core features of Kleefstra syndrome (KS). The reduction of Ehmt1 protein in *Ehmt1*$^{+/-}$ mice led to diminished H3K9 dimethylation at promoter regions of bone tissue related genes. Since expression of *Runx2*, *Col22a1*, *Col11a1*, and *Dmp1* mRNA was enhanced, the cranial abnormalities observed in *Ehmt1*$^{+/-}$ mice are likely caused by disturbed regulation of bone tissue morphogenesis.

In KS patients developmental delay has been described as speech delay or absence, delayed motor development, late eruption of milk teeth, delayed eye contact and smiles, and delayed growth rate (Stewart and Kleefstra, 2007; Kleefstra syndrome Leaflet "Unique", 2009; Kleefstra et al., 2009). In agreement with this, we noted a significant delay of ear and eye opening, upper incisor eruption, and postnatal growth in *Ehmt1*$^{+/-}$ mice. The latter observation of reduced body weight and growth is in line with the fatal growth retardation of full knockout *Ehmt1*$^{-/-}$ embryo's (Tachibana et al., 2005). In addition, we recently reported that Ehmt1 protein levels in wildtype mice were relatively high at postnatal day 4, declined to 50% at P8, and diminished further to 10% of the original P4 level by the time the animals were 1 month old (Balemans et al., 2013), indicating an important role for Ehmt1 in early postnatal development. Ehmt1 protein levels remained at the 1 mo level when at 3 or 10 months of age, and, importantly, the heterozygous *Ehmt1*$^{+/-}$ mice revealed a ~50% Ehmt1 protein reduction at all postnatal and adult times analyzed (Balemans et al., 2013). Postnatal reduction of Ehmt1 likely will affect brain and body development.

Both delayed motor development and childhood hypotonia are characteristics of KS patients (Stewart and Kleefstra, 2007; Kleefstra syndrome Leaflet "Unique", 2009; Kleefstra et al., 2009). Accordingly, in *Ehmt1*$^{+/-}$ mouse pups we observed delays in reaching mature levels in two motor function tests, reduced bar holding times, and shaking/unstable walking behavior. Notably, these motor function deficits were absent in the adult *Ehmt1*$^{+/-}$ mice (Balemans et al., 2010, 2013).

In-depth analysis of cranial morphology revealed brachycephaly, a shorter nasal bone, and hypertelorism in *Ehmt1*$^{+/-}$ mice, thereby recapitulating the cranial abnormalities observed in KS patients (Stewart and Kleefstra, 2007; Kleefstra syndrome Leaflet "Unique", 2009; Kleefstra et al., 2009). Similarly, mouse models for Down syndrome and Apert syndrome, or with *Tcf12* or *Erf* haploinsufficiency, mimicked the patient's craniofacial characteristics (Richtsmeier et al., 2000; Wang et al., 2005; Yin et al., 2008; Sharma et al., 2013; Twigg et al., 2013). The observation that 35% of the adult *Ehmt1*$^{+/-}$ crania showed a bent nose, as opposed to 0% for adult wildtypes, is in line with the craniofacial asymmetry noted in at least one patient with KS (Kleefstra et al., 2009). *Twist1*, *Fgfr2*, *Frem1*, *Tcf12, Erf, Satb2 and Il11ra* mutant mouse models for craniosynostosis display a similar bent-nose phenotype and/or brachycephaly due to abnormal suture fusion (Bourgeois et al., 1998; Yin et al., 2008; Vissers et al., 2011; Fish et al., 2011; Nieminen et al., 2011; Sharma et al., 2013; Twigg et al., 2013). Notably, in *Fgfr3*^{P244R} mice the direction of nose deviation correlated with ipsilateral fusion of the premaxillary suture (Twigg et al., 2009). Another study in rats revealed that unilateral artificial synostosis of the premaxillary suture caused the nose to bend toward the treated side (Xenakis et al., 1995). However, in the adult *Ehmt1*$^{+/-}$ mice with a bent nose, the premaxillary suture on the left or the right side did not seem to be altered (CEEM Van der Zee, own observations).

The posterior frontal suture, analogous to the metopic suture in humans, physiologically closes between postnatal day 25–45 in mice (Bradley et al., 1996). However, various studies reported that this suture can remain patent later in life in both humans and mice (Cohen, 1993; Recinos et al., 2004; Stadler et al., 2006). This was demonstrated by the fact that only 15% of the wildtype mice displayed a patent posterior frontal suture. Interestingly, patency was observed in a significantly higher percentage (75%) of *Ehmt1*$^{+/-}$ mice. The Apert syndrome *Fgfr2*$^{+/S252W}$ (Wang et al., 2005) and Fgfr2 *Fgfr2*$^{+/P253R}$ (Yin et al., 2008) mice show also patency of the posterior frontal suture, with synostosis of the coronal and sagittal sutures.

Bone formation is a tightly regulated process with multiple factors controlling proliferation of osteogenic stem cells and their differentiation during bone morphogenesis (Komori, 2010; Miraoui et al., 2010). In this context, it is of major interest that the P28 *Ehmt1*$^{+/-}$ mice showed significantly increased expression of *Runx2* mRNA, and enhanced Runx2 immunostaining, in their skull bone. This multifunctional transcription factor Runx2 controls bone development by regulating the differentiation of osteoblasts and the expression of bone matrix protein genes during embryonic development and in the postnatal period (Ducy et al., 1999; Komori, 2010; Maeno et al., 2011). In addition, Runx2 needs to be downregulated in the final phase of bone maturation, indicating the delicate balance for Runx2 expression regulation (Maruyama et al., 2007; Komori, 2010). The observed increase of *Runx2* mRNA and protein in P28 *Ehmt1*$^{+/-}$ mice will affect this balance, which might explain the observed aberrant bone formation (Maeno et al., 2011; this study). Interestingly, the lack of

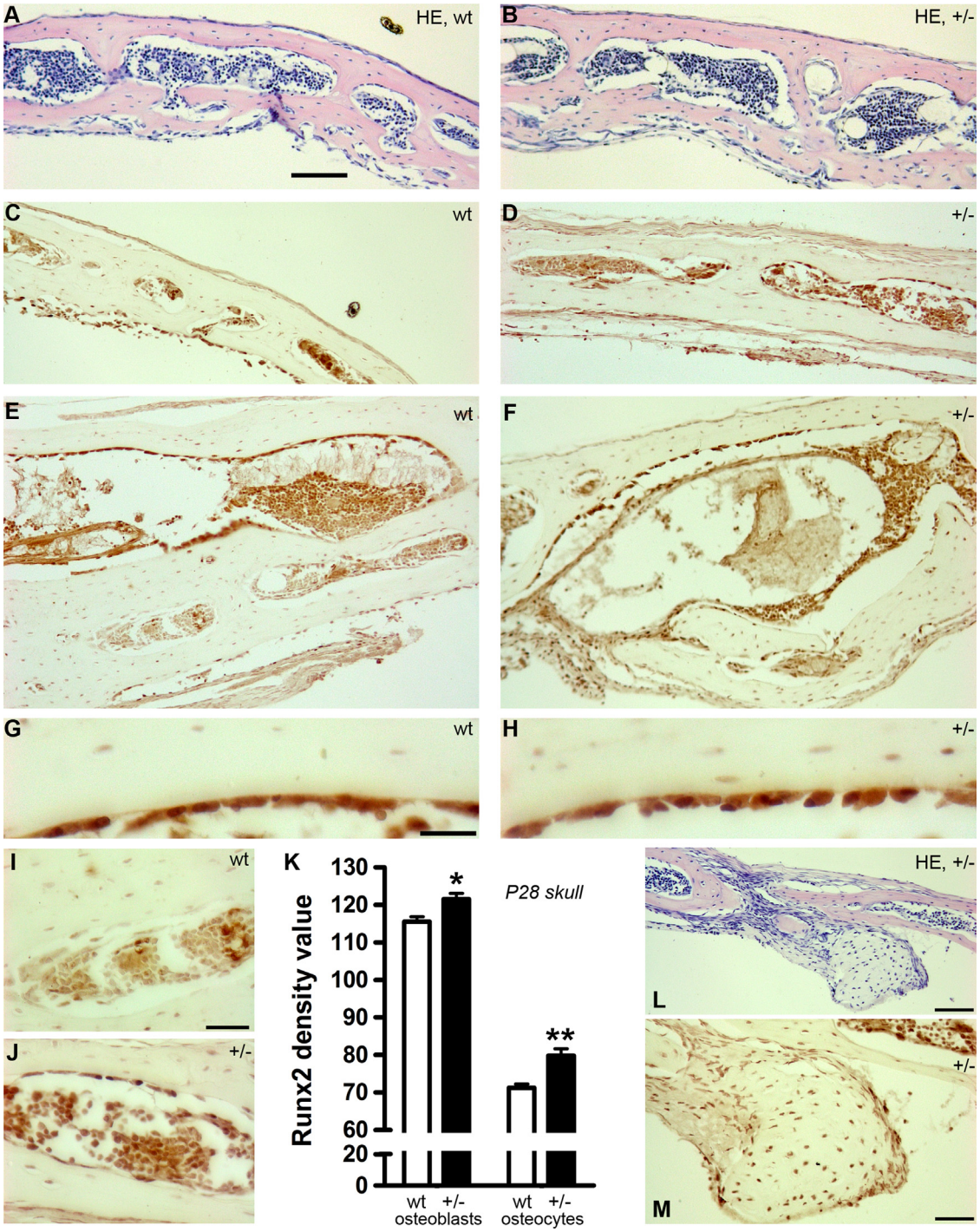

Fig. 8. Runx2 immunostaining of P28 skull bone sections. Haematoxylin and eosin (HE) histochemical staining visualized the characteristic double plate structure of skull bone, with the osteocytes in the bone matrix and osteoblasts in the space between the plates, in P28 wildtype (wt, (A)) and *Ehmt1*$^{+/-}$ ($^{+/-}$, (B)) mice. Immunostaining for Runx2 (C)–(J) and (M) indicated the presence of Runx2 protein in osteoblasts and osteocytes in skull bone tissue of P28 wildtype ((C), (E), (G), (I)) and *Ehmt1*$^{+/-}$ ((D), (F), (H) and (J)) mice. Shown are lateral ((C) and (D)) and more central ((E) and (F)) portions of coronally cut frontal skull bone sections. Note the dark Runx2 immunostaining density of the aligning osteoblasts in the enlarged photographs for wildtype (G) and *Ehmt1*$^{+/-}$ (H). Osteocytes contained a lighter Runx2 density as shown for wildtype (I) and *Ehmt1*$^{+/-}$ (J). Quantification of Runx2 immunostaining density demonstrated significantly higher values for *Ehmt1*$^{+/-}$ osteoblasts ($^{*}p < 0.005$) and osteocytes ($^{**}p < 0.001$), compared to wildtype (K). Ectopic bone/cartilage was observed underneath the P28 *Ehmt1*$^{+/-}$ skull as shown with haematoxylin and eosin (L), and with a strong Runx2 staining in the cells (M). Bar in (A) (for (A)–(F)), 80 μm; bar in (G) (for (G), (H)), 20 μm; bar in (I) (for (I) and (J)), 20 μm; bar in (L), 80 μm; bar in (M), 40 μm.

changes in bone genes mRNA expression in P8 *Ehmt1*$^{+/-}$ mice is in line with the observation that these P8 *Ehmt1*$^{+/-}$ mice do not contain a bent nose (yet). Importance of correct Runx2 balance has been found in humans and mice. In humans, haploinsufficiency for *RUNX2* indeed caused cleidocranial dysplasia associated with defective calvarial ossification (Mundlos et al., 1997). After targeted disruption of *Cbfa1*/*Runx2* in mice complete lack of bone formation was reported, due to maturational arrest of the osteoblasts (Komori et al., 1997).

The mechanism behind the observed increased mRNA expression is likely related to H3K9 methylation, a hallmark of transcriptional repression (Hublitz et al., 2009). The Ehmt1/Ehmt2 (GLP/

G9a) complex mediates H3K9me2 to silence transcription (Tachibana et al., 2008). The *Ehmt1*$^{+/-}$ mice have ~50% reduction in Ehmt1 protein levels (Balemans et al., 2013), which correlated with the diminished H3K9me2 levels at several bone gene promoter sites in brain tissue, thereby explaining increased mRNA expression. Pharmacological inhibition of the Ehmt1(GLP)/Ehmt2 (G9a) complex also revealed decreased H3K9me2 levels (in this case at *Zif268* and *BDNF* exon IV gene promoters) concomitant with increased mRNA expression (Gupta-Agarwal et al., 2012). Notably, postnatal and neuron-specific ablation of *Ehmt1* (GLP)/ *Ehmt2*(G9a) led to derepression of nonneuronal genes in brain (Schaefer et al., 2009).

In addition to *Runx2*, the mRNA levels of *Col22a1*, *Col11a1* and *Dmp1* were also significantly increased in cranial bone tissue of the *Ehmt1*$^{+/-}$ mice. The minor fibrillar collagen Col11a1 is essential for skeletal bone morphogenesis (Li et al., 1995), whereas Col22a1 is present specifically at tissue junctions, is associated with the extrafibrillar matrix in cartilage, and can act as cell adhesion ligand for fibroblasts (Koch et al., 2004). Dmp1, dentin matrix acidic phosphoprotein 1, might indirectly promote osteoblast differentiation (Eapen et al., 2010), but is certainly critical for proper bone matrix mineralization during bone maturation (Rios et al., 2005; Toyosawa et al., 2001). Thus Col11a1, Col22a1, and Dmp1 all play a role in the formation of bone tissue. The enhanced *Dmp1* mRNA expression might be regulated through lower Ehmt1 activity, although H3K9me2 levels at the Dmp1 promotor site were not altered. A more likely explanation is an indirect regulation of Dmp1 by enhanced Runx2 levels, since this transcription factor regulates the expression of many bone tissue associated proteins like osteopontin, Col1a1, Col10a1, and Dmp1 (Komori, 2010).

In summary, the *Ehmt1*$^{+/-}$ mice recapitulate the core features of Kleefstra syndrome with intellectual disability, autistic-like features (Balemans et al., 2010, 2013), developmental delay, hypotonia, and cranial dysmorphisms (this study). Furthermore, the increased expression of bone tissue genes, and particularly Runx2, in P28 *Ehmt1*$^{+/-}$ crania likely contributed to the craniofacial phenotype of bent nose and brachycephaly in the *Ehmt1*$^{+/-}$ mouse model for Kleefstra syndrome, and can be explained by less gene silencing due to diminished Ehmt1-induced H3K9 dimethylation.

Acknowledgements

We want to thank M. Tachibana and Y. Shinkai for providing the *Ehmt1*$^{+/-}$ mice, T. Peters, L. Driessen, and J. Derken for assistance with bone tissue experiments, R. Wansink and W. Hendriks for critical reading of the manuscript, and the employees of the Central Animal Facility in Nijmegen for their help, advice, and animal care. This work was supported by the EU FP7 large-scale integrated project GENCODYS (grant 241995) to HvB, the Dutch brain foundation, KS 2009(1)-122 to TK, a fellowship from the Higher Education Commission (HEC) Pakistan to MA, and a grant from the Radboud University Nijmegen Medical Centre (Junior-onderzoekerronde 2007) to HvB and CEEMVdZ.

Appendix A. Supporting information

Supplementary data associated with this article can be found in the online version at http://dx.doi.org/10.1016/j.ydbio.2013.12.016.

References

Balemans, M.C., Huibers, M.M., Eikelenboom, N.W., Kuipers, A.J., van Summeren, R. C., Pijpers, M.M., Tachibana, M., Shinkai, Y., van Bokhoven, H., Van der Zee, C.E., 2010. Reduced exploration, increased anxiety, and altered social behavior: Autistic-like features of euchromatin histone methyltransferase 1 heterozygous knockout mice. Behav. Brain Res. 208, 47–55.

Balemans, M.C., Kasri, N.N., Kopanitsa, M.V., Afinowi, N.O., Ramakers, G., Peters, T.A., Beynon, A.J., Janssen, S.M., van Summeren, R.C., Eeftens, J.M., Eikelenboom, N., Benevento, M., Tachibana, M., Shinkai, Y., Kleefstra, T., van Bokhoven, H., Van der Zee, C.E., 2013. Hippocampal dysfunction in the Euchromatin histone methyltransferase 1 heterozygous knockout mouse model for Kleefstra syndrome. Hum. Mol. Genet. 22, 852–866.

Barski, A., Cuddapah, S., Cui, K., Roh, T.Y., Schones, D.E., Wang, Z., Wei, G., Chepelev, I., Zhao, K., 2007. High-resolution profiling of histone methylations in the human genome. Cell 129, 823–837.

Bourgeois, P., Bolcato-Bellemin, A.L., Danse, J.M., Bloch-Zupan, A., Yoshiba, K., Stoetzel, C., Perrin-Schmitt, F., 1998. The variable expressivity and incomplete penetrance of the twist-null heterozygous mouse phenotype resemble those of human Saethre-Chotzen syndrome. Hum. Mol. Genet. 7, 945–957.

Bradley, J.P., Levine, J.P., Roth, D.A., McCarthy, J.G., Longaker, M.T., 1996. Studies in cranial suture biology: IV. Temporal sequence of posterior frontal cranial suture fusion in the mouse. Plast. Reconstr. Surg. 98, 1039–1045.

Chadman, K.K., Yang, M., Crawley, J.N., 2009. Criteria for validating mouse models of psychiatric diseases. Am. J. Med. Genet. B Neuropsychiatr. Genet. 150B, 1–11.

Cohen Jr., M.M., 1993. Sutural biology and the correlates of craniosynostosis. Am. J. Med. Genet. 47, 581–616.

Daily, D.K., Ardinger, H.H., Holmes, G.E., 2000. Identification and evaluation of mental retardation. Am. Fam. Physician. 61 (1059-67), 1070.

Ducy, P., Starbuck, M., Priemel, M., Shen, J., Pinero, G., Geoffroy, V., Amling, M., Karsenty, G., 1999. A Cbfa1-dependent genetic pathway controls bone formation beyond embryonic development. Genes Dev. 13, 1025–1036.

Eapen, A., Sundivakkam, P., Song, Y., Ravindran, S., Ramachandran, A., Tiruppathi, C., George, A., 2010. Calcium-mediated stress kinase activation by DMP1 promotes osteoblast differentiation. J. Biol. Chem. 285, 36339–36351.

Fish, J.L., Villmoare, B., Köbernick, K., Compagnucci, C., Britanova, O., Tarabykin, V., Depew, M.J., 2011. Satb2, modularity, and the evolvability of the vertebrate jaw. Evol. Dev. 13, 549–564.

Gupta-Agarwal, S., Franklin, A.V., Deramus, T., Wheelock, M., Davis, R.L., McMahon, L.L., Lubin, F.D., 2012. G9a/GLP histone lysine dimethyltransferase complex activity in the hippocampus and the entorhinal cortex is requires for gene activation and silencing during memory consolidation. J. Neurosci. 32, 5440–5453.

He, H., Lehming, N., 2003. Global effects of histone modifications. Brief. Funct. Genomics Proteomics 2, 234–243.

Hublitz, P., Albert, M., Peters, A.H., 2009. Mechanisms of transcriptional repression by histone lysine methylation. Int. J. Dev. Biol. 53, 335–354.

Iwakoshi, M., Okamoto, N., Harada, N., Nakamura, T., Yamamori, S., Fujita, H., Niikawa, N., Matsumoto, N., 2004. 9q34.3 deletion syndrome in three unrelated children. Am. J. Med. Genet. A 126A, 278–283.

Kawakami, M., Yamamura, K., 2008. Cranial bone morphometric study among mouse strains. BMC Evol. Biol. 8, 73.

Kleefstra, T., Brunner, H.G., Amiel, J., Oudakker, A.R., Nillesen, W.M., Magee, A., Genevieve, D., Cormier-Daire, V., van Esch, H., Fryns, J.P., Hamel, B.C., Sistermans, E.A., de Vries, B.B., van Bokhoven, H., 2006. Loss-of-function mutations in euchromatin histone methyl transferase 1 (EHMT1) cause the 9q34 subtelomeric deletion syndrome. Am. J. Hum. Genet. 79, 370–377.

Kleefstra, T., van Zelst-Stams, W.A., Nillesen, W.M., Cormier-Daire, V., Houge, G., Foulds, N., van Dooren, M., Willemsen, M.H., Pfundt, R., Turner, A., Wilson, M., McGaughran, J., Rauch, A., Zenker, M., Adam, M.P., Innes, M., Davies, C., López, A. G., Casalone, R., Weber, A., Brueton, L.A., Navarro, A.D., Bralo, M.P., Venselaar, H., Stegmann, S.P., Yntema, H.G., van Bokhoven, H., Brunner, H.G., 2009. Further clinical and molecular delineation of the 9q subtelomeric deletion syndrome supports a major contribution of EHMT1 haploinsufficiency to the core phenotype. J. Med. Genet. 46, 598–606.

Kleefstra syndrome Leaflet "Unique", 2009. ⟨www.rarechromo.org/forum/DisordersLeaflets.asp⟩.

Kleefstra, T., Nillesen, W.M., Yntema, H.G., 2010. Kleefstra syndrome. In: Pagon, R.A., Bird, T.D., Dolan, C.R., Stephens, K. (Eds.), SourceGeneReviews [Internet] Seattle (WA). University of Washington, Seattle.

Kleefstra, T., Kramer, J.M., Neveling, K., Willemsen, M.H., Koemans, T.S., Vissers, L.E., Wissink-Lindhout, W., Fenckova, M., van den Akker, W.M., Kasri, N.N., Nillesen, W.M., Prescott, T., Clark, R.D., Devriendt, K., van Reeuwijk, J., de Brouwer, A.P., Gilissen, C., Zhou, H., Brunner, H.G., Veltman, J.A., Schenck, A., van Bokhoven, H., 2012. Disruption of an EHMT1-associated chromatin-modification module causes intellectual disability. Am. J. Hum. Genet. 2012 91, 73–82.

Koch, M., Schulze, J., Hansen, U., Ashwodt, T., Keene, D.R., Brunken, W.J., Burgeson, R.E., Bruckner, P., Bruckner-Tuderman, L., 2004. A novel marker of tissue junctions, collagen XXII. J. Biol. Chem. 279, 22514–22521.

Komori, T., Yagi, H., Nomura, S., Yamaguchi, A., Sasaki, K., Deguchi, K., Shimizu, Y., Bronson, R.T., Gao, Y.H., Inada, M., Sato, M., Okamoto, R., Kitamura, Y., Yoshiki, S., Kishimoto, T., 1997. Targeted disruption of Cbfa1 results in a complete lack of bone formation owing to maturational arrest of osteoblasts. Cell 89, 755–764.

Komori, T., 2010. Regulation of bone development and extracellular matrix protein genes by RUNX2. Cell Tissue Res. 339, 189–195.

Kramer, J.M., Kochinke, K., Oortveld, M.A., Marks, H., Kramer, D., de Jong, E.K., Asztalos, Z., Westwood, J.T., Stunnenberg, H.G., Sokolowski, M.B., Keleman, K., Zhou, H., van, B.H., Schenck, A., 2011. Epigenetic regulation of learning and memory by *Drosophila* EHMT/G9a. PLoS Biol. 9, e1000569.

Li, Y., Lacerda, D.A., Warman, M.L., Beier, D.R., Yoshioka, H., Ninomiya, Y., Oxford, J.T., Morris, N.P., Andrikopoulos, K., Ramirez, F., 1995. A fibrillar collagen gene, Col11a1, is essential for skeletal morphogenesis. Cell 80, 423–430.
Livak, K.J., Schmittgen, T.D., 2001. Analysis of relative gene expression data using real-time quantitative PCR and the 2(-Delta Delta C(T)) Method. Methods 25, 402–408.
Maeno, T., Moriishi, T., Yoshida, C.A., Komori, H., Kanatani, N., Izumi, S., Takaoka, K., Komori, T., 2011. Early onset of Runx2 expression caused craniosynostosis, ectopic bone formation, and limb defects. Bone 49, 673–682.
Marks, H., Chow, J.C., Denissov, S., Françoijs, K.J., Brockdorff, N., Heard, E., Stunnenberg, H.G., 2009. High-resolution analysis of epigenetic changes associated with X inactivation. Genome Res. 19, 1361–1373.
Maruyama, Z., Yoshida, C.A., Furuichi, T., Amizuka, N., Ito, M., Fukuyama, R., Miyazaki, T., Kitaura, H., Nakamura, K., Fujita, T., Kanatani, N., Moriishi, T., Yamana, K., Liu, W., Kawaguchi, H., Nakamura, K., Komori, T., 2007. Runx2 determines bone maturity and turnover rate in postnatal bone development and is involved in bone loss in estrogen deficiency. Dev. Dyn. 236, 1876–1890.
Miraoui, H., Severe, N., Vaudin, P., Pages, J.C., Marie, P.J., 2010. Molecular silencing of Twist1 enhances osteogenic differentiation of murine mesenchymal stem cells: implication of FGFR2 signaling. J. Cell Biochem. 110, 1147–1154.
Mundlos, S., Otto, F., Mundlos, C., Mulliken, J.B., Aylsworth, A.S., Albright, S., Lindhout, D., Cole, W.G., Henn, W., Knoll, J.H., Owen, M.J., Mertelsmann, R., Zabel, B.U., Olsen, B.R., 1997. Mutations involving the transcription factor CBFA1 cause cleidocranial dysplasia. Cell 89, 773–779.
Nieminen, P., Morgan, N.V., Fenwick, A.L., Parmanen, S., Veistinen, L., Mikkola, M.L., van der Spek, P.J., Giraud, A., Judd, L., Arte, S., Brueton, L.A., Wall, S.A., Mathijssen, I.M., Maher, E.R., Wilkie, A.O., Kreiborg, S., Thesleff, I., 2011. Inactivation of IL11 signaling causes craniosynostosis, delayed tooth eruption, and supernumerary teeth. Am. J. Hum. Genet. 89, 67–81.
Recinos, R.F., Hanger, C.C., Schaefer, R.B., Dawson, C.A., Gosain, A.K., 2004. Microfocal CT: a method for evaluating murine cranial sutures in situ. J. Surg. Res. 116, 322–329.
Rice, J.C., Briggs, S.D., Ueberheide, B., Barber, C.M., Shabanowitz, J., Hunt, D.F., Shinkai, Y., Allis, C.D., 2003. Histone methyltransferases direct different degrees of methylation to define distinct chromatin domains. Mol. Cell 12, 1591–1598.
Richtsmeier, J.T., Baxter, L.L., Reeves, R.H., 2000. Parallels of craniofacial maldevelopment in Down syndrome and Ts65Dn mice. Dev. Dyn. 217, 137–145.
Rios, H.F., Ye, L., Dusevich, V., Eick, D., Bonewald, L.F., Feng, J.Q., 2005. DMP1 is essential for osteocyte formation and function. J. Musculoskelet. Neuronal Interact. 5, 325–327.
Schaefer, A., Sampath, S.C., Intrator, A., Min, A., Gertler, T.S., Surmeier, D.J., Tarakhovsky, A., Greengard, P., 2009. Control of cognition and adaptive behavior by the GLP/G9a epigenetic suppressor complex. Neuron 64, 678–691.
Sharma, V.P., Fenwick, A.L., Brockop, M.S., McGowan, S.J., Goos, J.A., Hoogeboom, A. J., Brady, A.F., Jeelani, N.O., Lynch, S.A., Mulliken, J.B., Murray, D.J., Phipps, J.M., Sweeney, E., Tomkins, S.E., Wilson, L.C., Bennett, S., Cornall, R.J., Broxholme, J., Kanapin, A., 2013. 500 Whole-Genome Sequences (WGS500) Consortium, Johnson D, Wall SA, van der Spek PJ, Mathijssen IM, Maxson RE, Twigg SR, Wilkie AO. Nat. Genet. 45, 304–307.
Stadler III, J.A., Cortes, W., Zhang, L.L., Hanger, C.C., Gosain, A.K., 2006. A reinvestigation of murine cranial suture biology: microcomputed tomography versus histologic technique. Plast. Reconstr. Surg. 118, 626–634.
Stewart, D.R., Kleefstra, T., 2007. The chromosome 9q subtelomere deletion syndrome. Am. J. Med. Genet. C Semin. Med. Genet. 145C, 383–392.
Tachibana, M., Matsumura, Y., Fukuda, M., Kimura, H., Shinkai, Y., 2008. G9a/GLP complexes independently mediate H3K9 and DNA methylation to silence transcription. EMBO J. 27, 2681–2690.
Tachibana, M., Ueda, J., Fukuda, M., Takeda, N., Ohta, T., Iwanari, H., Sakihama, T., Kodama, T., Hamakubo, T., Shinkai, Y., 2005. Histone methyltransferases G9a and GLP form heteromeric complexes and are both crucial for methylation of euchromatin at H3-K9. Genes Dev. 19, 815–826.
Toyosawa, S., Shintani, S., Fujiwara, T., Ooshima, T., Sato, A., Ijuhin, N., Komori, T., 2001. Dentin matrix protein 1 is predominantly expressed in chicken and rat osteocytes but not in osteoblasts. J. Bone Miner. Res. 16, 2017–2026.
Twigg, S.R., Healy, C., Babbs, C., Sharpe, J.A., Wood, W.G., Sharpe, P.T., Morriss-Kay, G.M., Wilkie, A.O., 2009. Skeletal analysis of the Fgfr3(P244R) mouse, a genetic model for the Muenke craniosynostosis syndrome. Dev. Dyn. 238, 331–342.
Twigg, S.R., Vorgia, E., McGowan, S.J., Peraki, I., Fenwick, A.L., Sharma, V.P., Allegra, M., Zaragkoulias, A., Sadighi Akha, E., Knight, S.J., Lord, H., Lester, T., Izatt, L., Lampe, A.K., Mohammed, S.N., Stewart, F.J., Verloes, A., Wilson, L.C., Healy, C., Sharpe, P.T., Hammond, P., Hughes, J., Taylor, S., Johnson, D., Wall, S.A., Mavrothalassitis, G., Wilkie, A.O., 2013. Reduced dosage of ERF causes complex craniosynostosis in humans and mice and links ERK1/2 signaling to regulation of osteogenesis. Nat. Genet. 45, 308–313.
van der Meer, M., Costa, P., Baumans, V., Olivier, B., Van Zutphen, L., 1999. Welfare assessment of transgenic animals: Behavioural responses and morphological development of newborn mice. Altern. Lab. Anim. 27, 857–868.
Vissers, L.E., Cox, T.C., Maga, A.M., Short, K.M., Wiradjaja, F., Janssen, I.M., Jehee, F., Bertola, D., Liu, J., Yagnik, G., Sekiguchi, K., Kiyozumi, D., van Bokhoven, H., Marcelis, C., Cunningham, M.L., Anderson, P.J., Boyadjiev, S.A., Passos-Bueno, M. R., Veltman, J.A., Smyth, I., Buckley, M.F., Roscioli, T., 2011. Heterozygous mutations of FREM1 are associated with an increased risk of isolated metopic craniosynostosis in humans and mice. PLoS Genet. 7, e1002278.
Wang, Y., Xiao, R., Yang, F., Karim, B.O., Iacovelli, A.J., Cai, J., Lerner, C.P., Richtsmeier, J.T., Leszl, J.M., Hill, C.A., Yu, K., Ornitz, D.M., Elisseeff, J., Huso, D.L., Jabs, E.W., 2005. Abnormalities in cartilage and bone development in the Apert syndrome FGFR2(+/S252W) mouse. Development 132, 3537–3548.
Willemsen, M.H., Vulto-van Silfhout, A.T., Nillesen, W.M., Wissink-Lindhout, W.M., van Bokhoven, H., Philip, N., Berry-Kravis, E.M., Kini, U., van Ravenswaaij-Arts, C. M., Delle Chiaie, B., Innes, A.M., Houge, G., Kosonen, T., Cremer, K., Fannemel, M., Stray-Pedersen, A., Reardon, W., Ignatius, J., Lachlan, K., Mircher, C., Helderman van den Enden, P.T., Mastebroek, M., Cohn-Hokke, P.E., Yntema, H.G., Drunat, S., Kleefstra, T., 2012. Update on Kleefstra syndrome. Mol. Syndromol. 2, 202–212.
Xenakis, D., Ronning, O., Kantomaa, T., Helenius, H., 1995. Reactions of the mandible to experimentally induced asymmetrical growth of the maxilla in the rat. Eur. J. Orthod. 17, 15–24.
Yin, L., Du, X., Li, C., Xu, X., Chen, Z., Su, N., Zhao, L., Qi, H., Li, F., Xue, J., Yang, J., Jin, M., Deng, C., Chen, L., 2008. A Pro253Arg mutation in fibroblast growth factor receptor 2 (Fgfr2) causes skeleton malformation mimicking human Apert syndrome by affecting both chondrogenesis and osteogenesis. Bone 42, 631–643.